ACS APPLIED MATERIALS & INTERFACES

Research Article

www.acsami.org

One-Step Pyrolytic Synthesis of Nitrogen and Sulfur Dual-Doped Porous Carbon with High Catalytic Activity and Good Accessibility to Small Biomolecules

Weiwei Gao,[†] Xun Feng,[†] Tianyi Zhang,[‡] Hao Huang,[†] Jin Li,[†] and Wenbo Song*[,†]

[†]College of Chemistry, Jilin University, 2699 Qianjin Street, Changchun 130012, China

[‡]College of Letters and Science, University of Wisconsin—Madison, 1305 Linden Drive, Madison, Wisconsin 53706, United States

Supporting Information

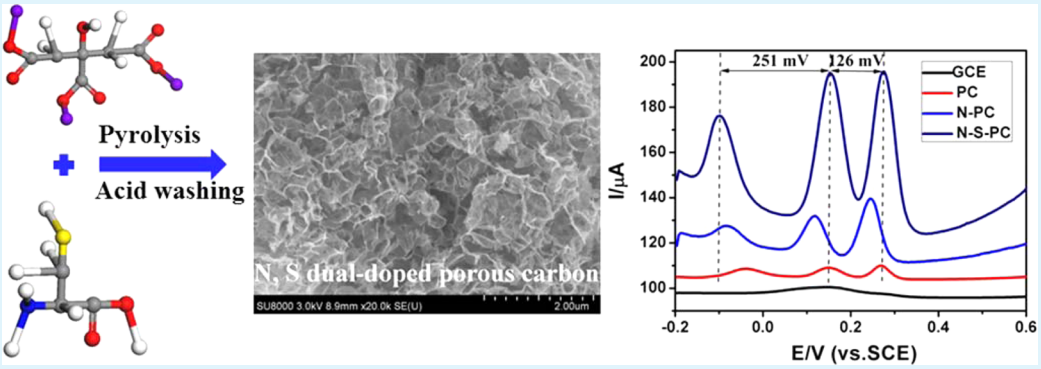

ABSTRACT: As one of promising catalysts that contain high density of active sites, N doped carbons have been extensively researched, while the reports for N, S dual-doped carbon materials are far less exhaustive. Herein, devoid of activation process and template, N, S dual-doped porous carbon (N−S−PC) was prepared for the first time via one-step pyrolysis of sodium citrate and cysteine. Possessing unique porous structure and large pore volume as well as good accessibility, N−S−PC demonstrates significantly improved electrocatalytic activity toward oxidation of ascorbic acid (AA), dopamine (DA), and uric acid (UA). In the coexisting system, the peak potential separation between AA and DA is up to 251 mV, which is much larger than for most of the other carbons. On the basis of large potential separation and high current response, selective and sensitive simultaneous determination of AA, DA, and UA was successfully accomplished by differential pulse voltammetry, displaying a linear response from 50 to 2000 μM, from 0.1 to 50 μM, and from 0.1 to 50 μM with a detection limit (S/N = 3) of 0.78, 0.02, and 0.06 μM. This work highlights the importance of N, S dual doping and hierarchical porous carbons for efficient catalysis.

KEYWORDS: *one-step pyrolysis, N, S dual-doping, porous carbon, electrocatalysis*

INTRODUCTION

Recent investigation reveals that doping of heteroatoms into carbon materials is an efficient method to enhance electrocatalytic performances.[1] Among those, nitrogen (N) is reckoned as a peerless dopant. Upon introduction of more electronegative N atoms into sp^2 hybridized C frameworks, the electric property and chemical activity can be modified.[2−5] Wang et al. have demonstrated that the spin density and charge distribution of C atom can be influenced by the neighbor N dopants, which induces "activation region" on the carbon surface that may directly participate in catalytic reactions.[6] Complementing N element, sulfur (S) is receiving increasing attention in carbon materials research very recently. As is known, N is preferential in tuning electronic properties of the carbon materials, whereas S is easy to polarize because of large lone pairs, inducing high chemical reactivity of the carbon materials.[7,8] Furthermore, recent density functional theory (DFT) calculation highlights the importance of changing spin density via S doping in catalysis.[9,10] More importantly, N, S dual doping may induce redistribution of spin and charge densities, providing a large number of active sites favorable for high catalytic activity.[7,8,11,12]

Meanwhile, porous carbons with hierarchical pore structure, large pore volume, and high specific surface area are viewed as promising materials for electrocatalytic reaction.[13,14] The mesopores can effectively facilitate diffusion of electrolyte ions to access the available surface area, whereas the macropores may act as ion buffers to ensure adequate penetration of the electrolyte into the electrode materials.[15] Therefore, incorporation of N, S atoms into porous carbon structures is promising for efficient catalysis. Nevertheless, N, S dual-doped porous carbons have rarely been reported to date.

Received: July 31, 2014
Accepted: October 17, 2014
Published: October 17, 2014

Scheme 1. Illustration of the Preparation Process of N−S−PC

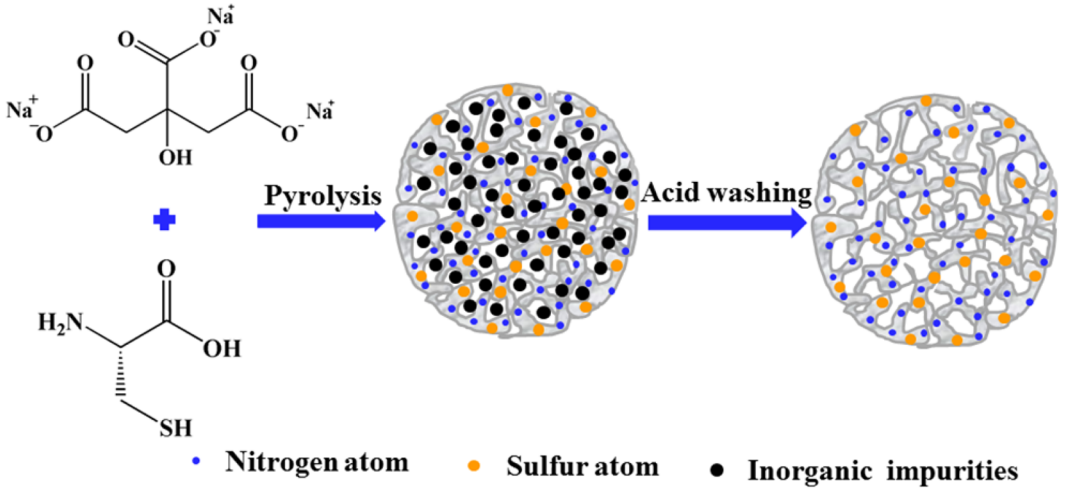

For example, Liu et al. described successful fabrication of 3D S−N co-doped carbon foam, which displayed pronounced oxygen reduction performance.[16] In this work, tedious processes including ultrasonic dispersion, evaporation-drying, annealing at high temperature, and removal of templates by HF etching were all involved. Qiao et al. recently synthesized two kinds of N, S dual doped hierarchical porous carbons with excellent specific capacitance and rate performance via a caustic KOH activation process.[15] Despite the progress in synthesizing N, S dual doped porous carbons, the current strategies are limited and still far from satisfactory in terms of simplicity and environmental benign.[8] Development of a facile and sustainable approach to achieve N, S dual doped porous carbon with abundant active sites, excellent electron, and reactant transfer rate is highly desired.

Free of template and chemical activation process, a feasible strategy emerges very recently to produce highly porous carbon via simple pyrolysis of alkali organic salts. During heat treatment of alkali organic salt, certain species are generated. These species are equivalent to activating agents to produce highly porous structure.[17] Upon introduction of a N, S-containing precursor, dual-doped porous carbon may be achieved via a developed one-step pyrolytic approach. Benefiting from the dual doping effect and the unique porous structure, the resulting carbon material may possess high catalytic activity and facile mass transport property toward biomolecules.

Ascorbic acid (AA), dopamine (DA), and uric acid (UA) are important biospecies that play significant roles in the physiological function of metabolism, central nervous system, and circulation system of the human body. The deficiency or maladjustment of their levels may lead to symptoms of many diseases such as cancer, Parkinson's disease, and hyperuricemia.[18−20] Hence, simultaneous determination of AA, DA, and UA is of critical importance for developing nerve physiology, making diagnoses, and controlling medicine. However, conventional electrodes normally result in poor selectivity and low reproducibility. Various carbon-based materials have thus been proposed as electrode modifiers,[21−26] and heteroatom doped porous carbon is viewed as one of the promising electrode materials. To the best of our knowledge, dual-doped porous carbon for simultaneous determination of AA, DA, and UA has not been reported.

Herein, a one-step approach was proposed to synthesize N, S dual-doped porous carbon (N−S−PC) via co-pyrolysis of sodium citrate and cysteine. Cysteine, a constituent unit of organisms, acted as both nitrogen and sulfur sources. In situ N and S co-doping was initiated by heat treatment. After resolution of inorganic impurities, the N−S−PC was achieved. The promising application of N−S−PC as one of the high-performance electrocatalysts in simultaneous determination of AA, DA, and UA was demonstrated for the first time. The effect of N and S dual-doping on the electrocatalytic activity toward AA, DA, and UA was systematically studied.

EXPERIMENTAL SECTION

Reagents and Materials. Sodium citrate was purchased from Beijing Chemical Plant. Cysteine and hydrochloric acid were purchased from Tianjin Chemical Plant. DA, UA, AA were obtained from Shanghai Chemical Reagents Co. Ltd. All chemicals were of analytical grade and used as received without further purification. All solutions were prepared with ultrapure water prior to use.

Instrumentation. Electrochemical experiments were carried out on a CHI 660B electrochemical workstation (Shanghai ChenHua Instruments Co., China). A conventional three-electrode system was used, which consisted of a platinum wire as counter electrode, a saturated calomel electrode (SCE) as reference electrode, and the modified glassy carbon electrode (GCE, diameter of 3 mm) as working electrode. All electrochemical measurements were carried out in phosphate buffer solutions (PBS) at room temperature.

The morphologies of porous carbons were characterized using a scanning electron microscope (SEM) (Shimadzu SSX-550, Japan) and a transmission electron microscope (TEM) (JEOL 3010). X-ray diffraction (XRD) data were recorded on a Siemens D5005 diffractometer with Cu Kα radiation (λ = 1.5406 Å). X-ray photoelectron spectroscopy (XPS) was performed on a Thermo Electron Corporation spectrometer with an Al Kα = 300.0 eV excitation source. Raman spectra were recorded at ambient temperature on a Renishaw Raman system model 1000 spectrometer with an argon-ion laser at an excitation wavelength of 532 nm. The nitrogen adsorption−desorption curve was measured using a N_2 adsorption apparatus (BELSORP-max, Japan).

Preparation of Carbon Samples. In a typical procedure, sodium citrate and cysteine powder with a mass ratio of 10:1 were first ground uniformly and then transferred into a porcelain boat. After flushing with N_2 flow for 2 h, the mixture was further heated in a horizontal tube furnace up to 800 °C at a rate of 3 °C min^{-1} and maintained for 1 h under N_2 flow. The pyrolysis products were purified with diluted hydrochloric acid to remove the inorganic impurities, followed by washing with adequate ultrapure water until the filtrate was neutral.

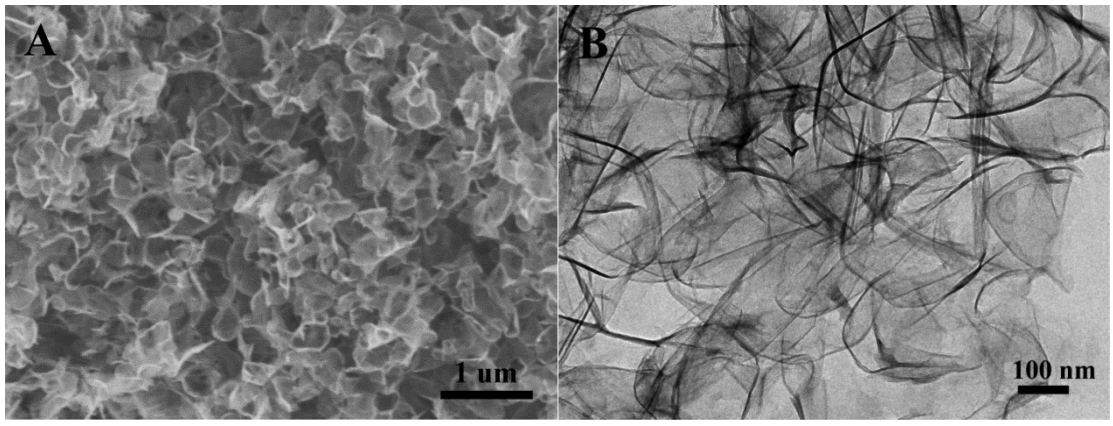

Figure 1. SEM (A) and TEM (B) images of N−S−PC.

Finally, the carbon sample was dried under vacuum at 120 °C for 12 h. In addition, three carbon materials were also prepared under the same thermal treatment condition as the control. The N-doped porous carbon (N−PC) was obtained with alanine and sodium citrate as starting materials. The N, S dual-doped carbon without porous structure (N−S−C) and nondoped porous carbon (PC) were synthesized via solely pyrolysis of cysteine and sodium citrate, respectively.

Preparation of Working Electrodes. Prior to modification, the GCE was carefully polished to a mirror-like plane with 0.3 and 0.05 μm alumina slurries. Afterward, the electrode was rinsed thoroughly with ultrapure water and ethanol alternatively in an ultrasonic bath, followed by drying under N_2 atmosphere. The N−S−PC modified GCE (N−S−PC/GCE) was prepared by casting 5 μL of N−S−PC suspension (1 mg mL^{-1} N−S−PC in *N*,*N*-dimethylformamide) on the surface of GCE and dried at room temperature for 24 h. For comparison, the N−PC/GCE, N−S−C/GCE, and PC/GCE were also prepared using the same procedure.

RESULTS AND DISCUSSION

Characterization of Porous Carbon Samples. Porous carbon samples were prepared via a feasible direct-synthesis approach, which is schematically shown in Scheme 1. During the pyrolysis, sodium citrate decomposes to sodium and sodium compounds, which operate as activating agents similar to KOH or NaOH.[17] Accompanying intercalation of sodium vapors between the carbon nanosheets, the decomposition products of cysteine are in situ incorporated, causing swelling and disruption of the carbon microstructure. After the inorganic impurities are washed with diluted hydrochloric acid, the open porous structure is developed, which can be well-observed by SEM characterization (Figure 1A). The resultant carbon exhibits spongelike morphology with many large pores of several hundred nanometers in size, indicating that an effective activation process occurs during heat treatment of sodium citrate and cysteine. Similar morphologies with N−S−PC are also observed for N−PC and PC (Figure S1A,C), while for N−S−C (Figure S2A,B), nonporous irregular bulk morphology is observed, confirming the effective activation of sodium salt. The porous structures of N−S−PC, N−PC, and PC were also confirmed by TEM. As shown in Figure 1B, Figure S1B, and S1D, the carbons display irregular wrinkled structure with curvature of the carbon nanosheets. The N−S−PC exhibits more scrolling and corrugation, arising potentially from the defective structures formed by N, S dual doping.[7]

The X-ray diffraction (XRD) patterns of porous carbons recorded at low scan rate are shown in Figure 2A. The

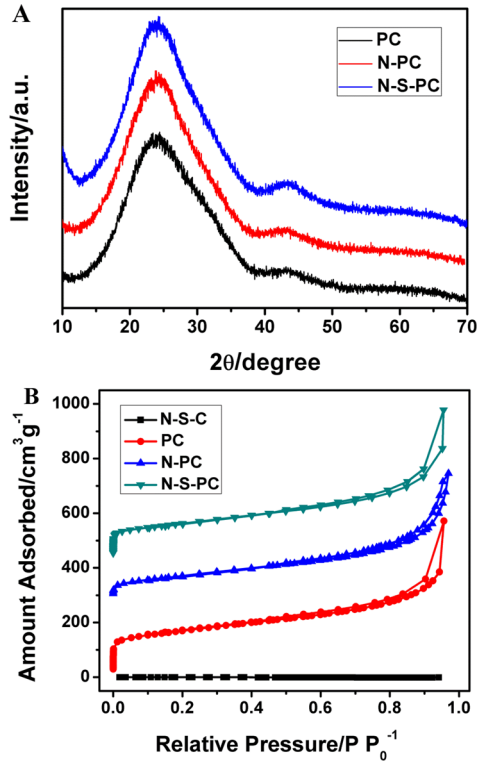

Figure 2. X-ray diffraction patterns (A) and nitrogen adsorption−desorption curves (B) of the as-prepared samples.

comparative XRD data of the N−S−C sample are also collected and shown in Figure S3. All the porous carbon samples display similar diffraction features. Two wide diffraction peaks located at around 23° and 43.5° are observed, which are the equivalent of hexagonal graphite 002 (2θ = 26°) and 100 (2θ = 43°) reflections, respectively. The interlayer spacing of the (002) plane of both samples is much larger than that of the graphite crystal structure with 0.34 nm. The enlarged interlayer spacing is believed favorable for the diffusion of reactants in electrolyte.[27,28] These features indicate that the porous carbon materials are disordered or amorphous.

A nitrogen adsorption−desorption analysis can prove the developed porous structure. As shown in Figure 2B, PC, N−PC, and N−S−PC samples all exhibit typical IV isotherms with pronounced hysteresis loops in the medium- and high-pressure regions. The pore characterizations of all the synthesized

dx.doi.org/10.1021/am505080r | ACS Appl. Mater. Interfaces 2014, 6, 19109−19117

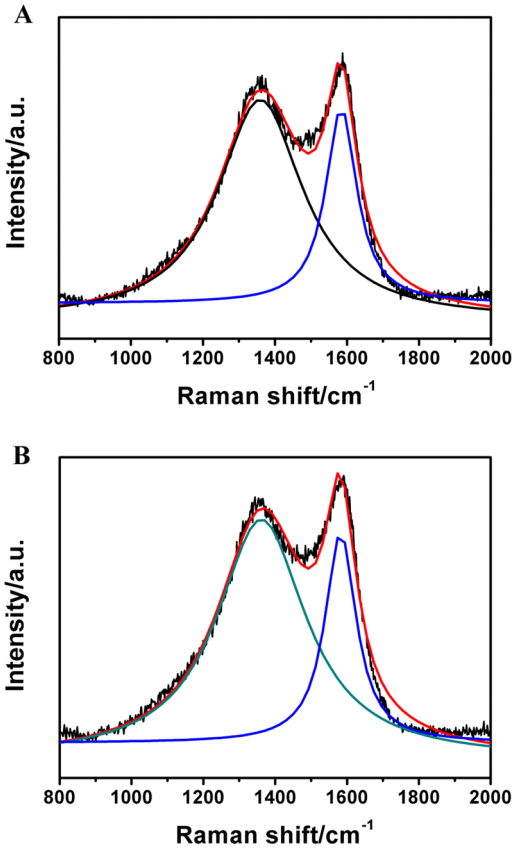

Figure 3. Raman spectra of PC (A) and N−S−PC (B).

materials are compiled in Table S1. It is worth noting that the N−S−C sample shows almost no porosity, having a very low pore volume and surface area, which is consistent with the SEM image, while the other samples exhibit dramatically enlarged pore volume as well as high surface area. Compared with PC, the BET surface area of N−S−PC slightly decreases because of N, S dual doping. However, the total pore volume is also as large as 2.5 cm^3 g^{-1}, which may facilitate mass transfer of molecules and ions in aqueous electrolyte.[25]

Further structural information on the samples was obtained by Raman spectra analysis. Figure 3 displays the Raman spectra of N−S−PC and PC. Two typical peaks at about 1350 and 1590 cm^{-1} are observed for all samples, corresponding to D and G bands, respectively. Generally, D band is commonly assigned to a breathing mode of A_{1g} symmetry that involves disordered carbon, edge defects, and other defects,. G band corresponds to the zone center of the E_{2g} mode, associated with phonon vibrations in sp^2 carbon materials.[29] Interestingly, compared to the G peak at 1592 cm^{-1} for PC, the N−S−PC manifests a down-shift of the G peak to 1585 cm^{-1}. This result further proves that N and S atoms have been successfully doped into the carbon material.[10] In addition, the N−S−PC displays relatively higher ratio of D band to G band (I_D/I_G) than PC (3.28 and 3.11, respectively). Since the value of I_D/I_G correlates with the disorder degree of carbon materials, this result indicates that more structural distortion was caused by N, S dual doping. Similar phenomena have been found in previous heteroatom-doped materials.[1,29]

The heteroatoms in N−S−PC were first probed by energy dispersive spectroscopy (EDS). Figure S4 reveals that C, N, S, and O elements all exist in the sample, and the distribution of

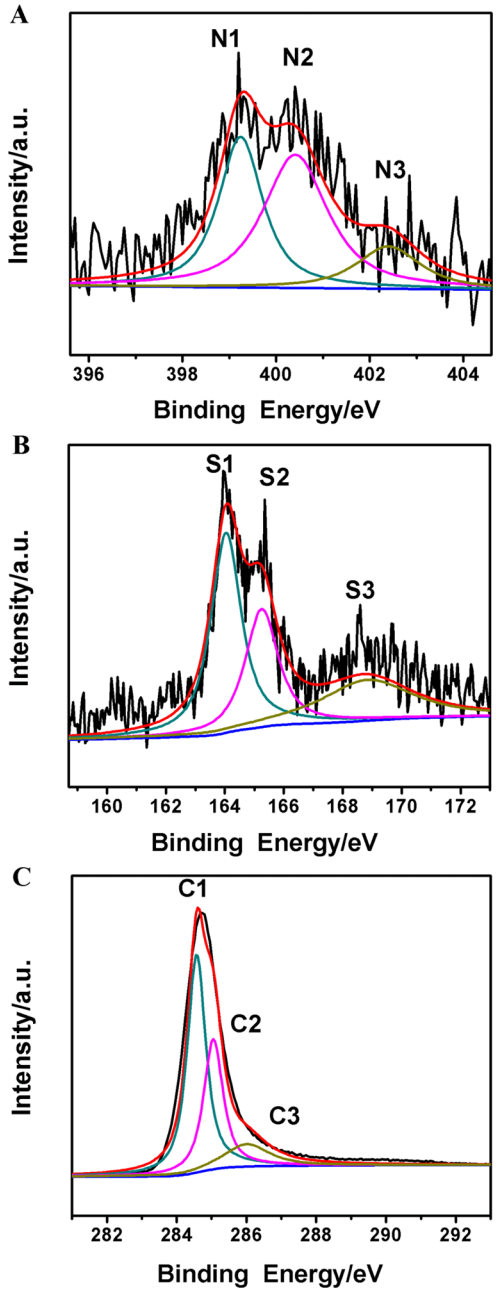

Figure 4. High resolution XPS spectra of N 1s (A), S 2p (B), and C 1s (C) of N−S−PC.

each element is homogeneous (Figure S5). To further investigate the chemical status of N and S atoms in N−S−PC, high resolution X-ray photoelectron spectroscopy (XPS) was performed. Figure 4 shows detailed scans of C 1s, N 1s, and S 2p orbitals. Two main peaks centered at 399.2 and 401.4 eV in Figure 4A refer to pyridinic-N (N1) and graphitic-N (N2), respectively, indicating that N atoms have been structurally integrated into the extended carbon network rather than presented as surface functionalities. An additional weak contribution at higher binding energy around 402 eV can be assigned to pyridinic N-oxide.[6] The N doping level in porous carbon is ∼2%, which is comparable to that of the N solely doped porous carbon as shown in Figure S6. The N binding configuration is mainly in the form of N1 and N2, which is believed favorable for enhancing electrochemical properties of

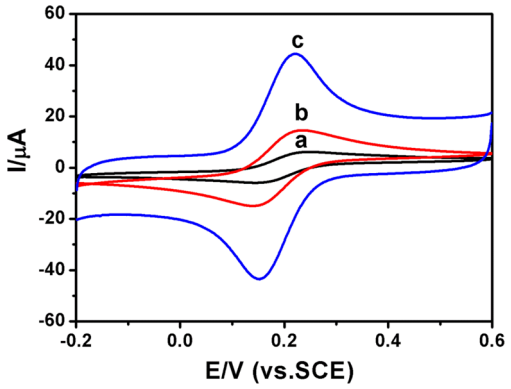

Figure 5. CVs obtained at GCE (a), PC/GCE (b), and N–S–PC/GCE (c) in 0.1 M PBS (pH 7.0) in 5 mM $Fe(CN)6^{3-/4-}$ + 0.1 M KCl aqueous solution at a scan rate of 50 mV s^{-1}.

porous carbon.[23] In the case of sulfur, relatively low doping level of 0.8% is achieved. High resolution S 1s spectra exhibit three peaks at the binding energies of 164.0, 165.2, and 168.8 eV, respectively (Figure 4B), similar to N–S–C (Figure S6). The former two peaks are in accordance with the S $2p_{3/2}$ (S1) and S $2p_{1/2}$ (S2) of –C–S–C– covalent bond of thiophene-S, owing to their spin–orbit couplings. The third weak peak (S3) should correspond to the sulfate (–C–SO_4–C–) or sulfonate (–C–SO_3–C–) (S3) in N–S–PC.[28,30] One can see that the S element is mainly doped at the edges and defects of carbon, existing in C–S–C bonds in thiophene-like structures with neighboring carbon atom.

Similarly, the C 1s spectrum can also be fitted into three peaks (Figure 4C). The intense peak at 284.6 eV is ascribed to the sp^2 hybridized graphitic carbon (C1), which indicates that most of the carbon atoms are arranged in a conjugated honeycomb lattice. This phenomenon is also observed in N–PC and N–S–C (Figure S6). The lower intensity peak at 285.1 eV is attributed to carbon atoms single-bonded to sulfur, nitrogen, or oxygen (C2), and the broad peak located at 286.1 eV corresponds to carbonyl or amide groups (C3) bonds.[11] Essentially, the XPS results coupled with Raman spectroscopy strongly confirm that N and S atoms have been successfully incorporated into carbon frameworks. Previous reports have proved that dual-doping of N and S introduces asymmetrical spin and charge density, which may bring a large number of active sites and provide enhanced electrocatalytic activity of the porous carbon materials.[7,29,31]

Electrochemistry and Electrocatalytic Oxidation of AA, DA, and UA. The electron transfer behavior and effective surface areas of various electrodes were evaluated by measuring the cyclic voltammograms (CVs) in 5 mM $K_3Fe(CN)_6$/0.1 M KCl solution. As displayed in Figure 5, the potential separation between anodic and cathodic peaks (ΔE_p) is 86 mV for PC/GCE, while N–S–PC/GCE shows a much smaller ΔE_p of 72 mV. Therefore, electron transfer at N–S–PC/GCE is more facile than that at PC/GCE, attributed to high electrical conductivity resulting from heteroatom doping.[25] The dramatic enhanced peak current at N–S–PC/GCE compared with those of PC/GCE and GCE suggests that N–S–PC possesses much more electrochemical active sites.

The individual electrochemical behavior of AA, DA, and UA at GCE, PC/GCE, N–PC/GCE, N–S–PC/GCE, and N–S–C/GCE was investigated by cyclic voltammetry (CV) (Figure 6 and Figure S7) and differential pulse voltammetry (DPV)

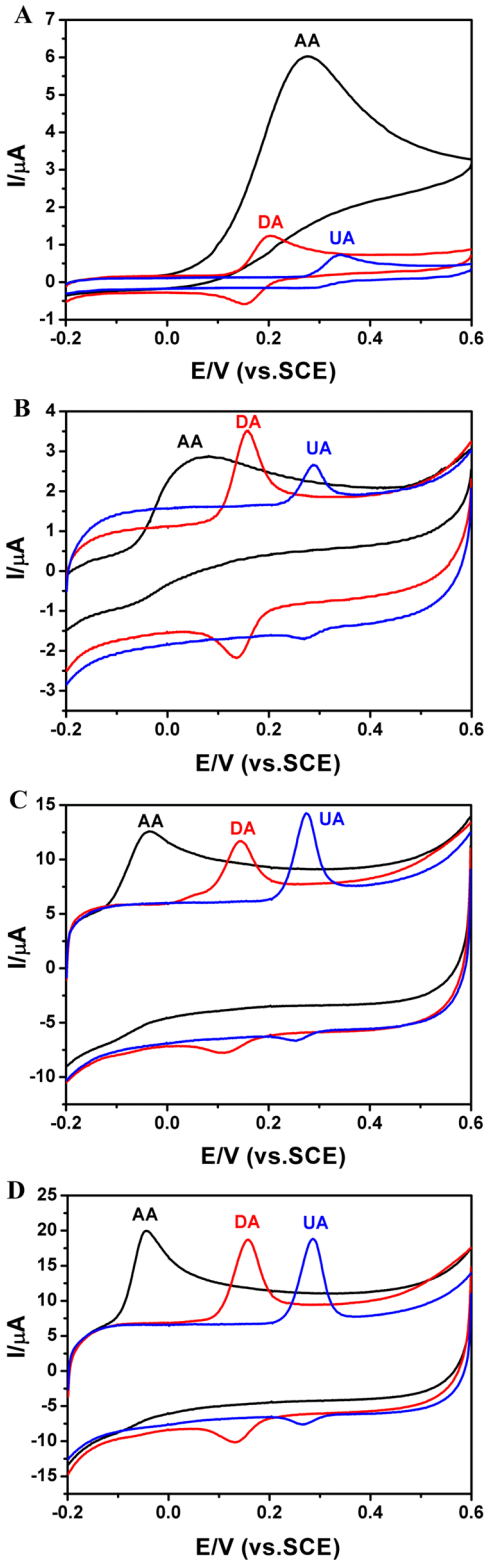

Figure 6. CVs of 400 μM AA, 15 μM DA, and 30 μM UA at GCE (A), PC/GCE (B), N–PC/GCE (C), and N–S–PC/GCE (D) in 0.1 M PBS (pH 7.0) at 50 mV s^{-1}.

(Figure S8), respectively. At GCE (Figure 6A), AA and UA show irreversible oxidation peaks at around 274.5 and 337 mV, respectively, while the cathodic and anodic peaks of DA appear at 148.7 and 205.5 mV, with ΔE_p of about 60 mV. It is thus difficult to distinguish AA, DA, and UA at GCE. Similar result is

dx.doi.org/10.1021/am505080r | ACS Appl. Mater. Interfaces 2014, 6, 19109–19117

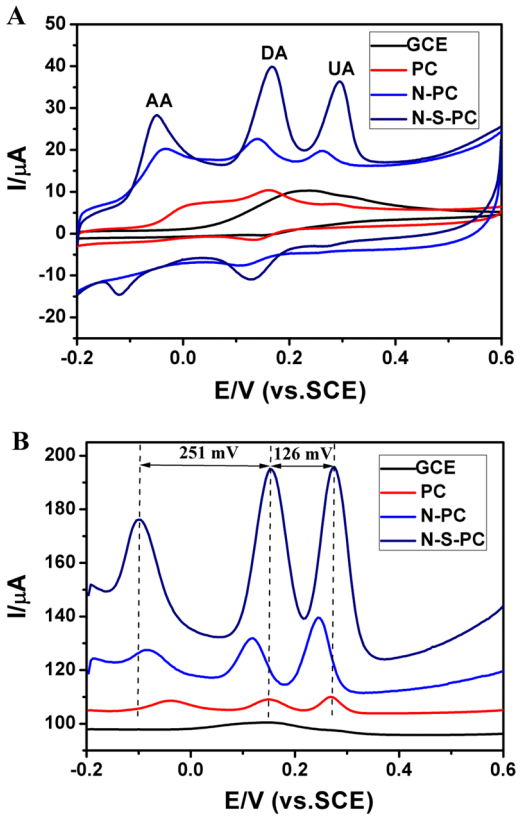

Figure 7. CVs (A) and DPVs (B) at GCE, PC/GCE, N−PC/GCE, and N−S−PC/GCE in 0.1 M PBS (pH 7.0) containing 600 μM AA, 20 μM DA, and 30 μM UA at 50 mV s^{-1}.

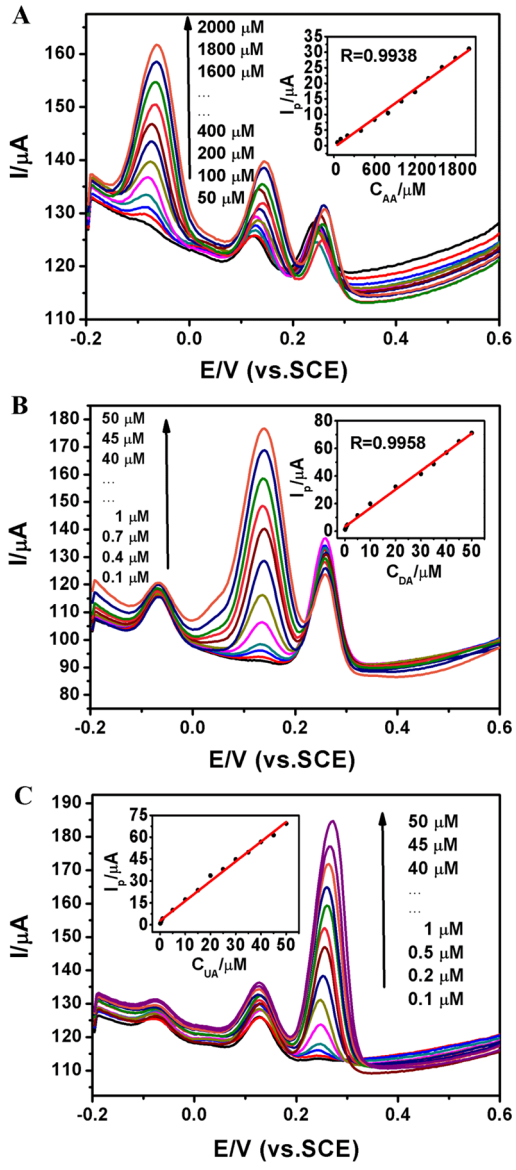

Figure 8. DPVs at N−S−PC/GCE in 0.1 M PBS (pH 7.0) (A) containing 3 μM DA, 4 μM UA, and different concentration of AA (from inner to outer): 50, 100, 200, 400, 600, 800, 1000, 1200, 1400, 1600, 1800, 2000 μM; (B) containing 600 μM AA, 8 μM UA, and different concentration of DA (from inner to outer) 0.1, 0.4, 0.7, 1, 5, 10, 20, 30, 35, 40, 45, 50 μM; (C) containing 600 μM AA, 5 μM DA, and different concentration of UA (from inner to outer) 0.1, 0.2, 0.5, 1, 5, 10, 15, 20, 25, 30, 35, 40, 45, 50 μM. Insets: plots of peak current I_p vs concentration for AA, DA, and DA, respectively.

also obtained at N−S−C/GCE (Figure S7), due to the difficulty of analyte transport in nonporous carbon. While at PC/GCE, N−PC/GCE, and N−S−PC/GCE (Figure 6B−D), the oxidation peak of AA negatively shifts. Especially for N−S−PC/GCE, the oxidation peak potential (−45 mV) is much more negative than that of PC/GCE (+50 mV) and N−PC/GCE (−34 mV). The DPV curves in Figure S8A also manifest similar trend, indicating enhanced catalytic activity of N−S−PC/GCE toward oxidation of AA. Moreover, the DPV peak current at N−S−PC/GCE reaches 28.0 μA, which is much higher than that of PC/GCE (3.37 μA) and GCE (3.84 μA). It is also 2.73 times as high as that of N−PC/GCE (10.25 μA). Previous work has demonstrated that more edge-active sites were produced upon S doping, resulting from the structural defects in the carbon crystal lattice due to the large atomic sizes of S. In addition, the possible interaction between lone pairs of sulfur with analyte may sufficiently generate profound effects on electrocatalytic activity, even though a small amount of S was doped.[8]

In the case of DA, a couple of well-defined redox peaks with a much smaller ΔE_p of 22.7 mV can be observed on N−S−PC/GCE. The reversibility of DA redox reaction at N−S−PC/GCE is much better than the other materials, which is even much better than those in some recent reports.[32,33] Meanwhile, the DPV peak current at N−S−PC/GCE is as high as 49.66 μA, which is much higher than that of N−PC/GCE, PC/GCE, and GCE (Figure S8B). For UA, a sharp oxidation peak and a broad reduction peak appear at various carbon materials, revealing an EC mechanism.[26] The DPV peak current at N−S−PC/GCE is 63.21 μA, which is 4, 14, and 23 times of that at N−PC/GCE (21.04 μA), PC/GCE (4.45 μA), and GCE (2.74 μA), respectively (Figure S8C).

To demonstrate the possibility of simultaneous determination of these biomolecules, the CV responses of AA, DA, and UA mixture are shown in Figure 7A and Figure S9A. At GCE and N−S−C/GCE, the oxidation peaks of AA, DA, and UA overlap with each other, resulting in only a small broad peak. The N−S−PC/GCE exhibits three sharp and well-defined oxidation peaks, with obvious enhanced peak separation and current in comparison with N−PC or PC. Furthermore, DPV was also performed to investigate the possibility of simultaneous determination of these biomolecules (Figure 7B and Figure S9B). Complete overlapping of the oxidation peaks at

dx.doi.org/10.1021/am505080r | ACS Appl. Mater. Interfaces 2014, 6, 19109−19117

Table 1. Comparison of the Analytical Performance of N−S−PC with Other Carbon-Based Materials in Simultaneous Determination of AA, DA, and UA

	peak separation (mV)		linear range (μM)			detection limit (μM)			
electrode materials	AA−DA	DA−UA	AA	DA	UA	AA	DA	UA	ref
N−PCNPs[a]	228	124	80−2000	0.5−30	4−50	0.74	0.011	0.021	23
NG	200	132	5−1300	0.5−170	0.1−20	2.2	0.25	0.045	24
HNCMS[b]	212	136	100−1000	5−70	3−30	0.027	0.93	0.59	25
HNCS-RGO[c]	252	132	50−1200	0.5−90	1−70	0.65	0.12	0.18	26
CNF[d]	190	150	2.0−64	0.04−5.6	0.8−16.8	2.00	0.04	0.20	34
Pt/MWCNT	166	120	24.5−765	0.06−2.03	0.46−50	20	0.048	0.35	35
chitosan−GR	165	90	50−1200	1−24	2−45	50	1	2	22
OMC/Nafion	190	150	40−800	1−90	5−80	20	0.5	4.0	21
N−S−PC	251	126	50−2000	0.1−50	0.1−50	0.78	0.02	0.06	this work

[a]Nitrogen-doped porous carbon nanopolyhedra. [b]Hollow-nitrogen-doped carbon microspheres. [c]Nitrogen-doped carbon-sphere-reduced graphene oxide. [d]Carbon nanofiber modified carbon paste electrode.

N−S−C/GCE and GCE suggests that simultaneous discrimination of these species is impossible. In contrast, three well resolved oxidation peaks are observed at −100.8, 150.2, and 276.2 mV on N−S−PC/GCE, corresponding to oxidation of AA, DA, and UA, respectively. The peak potential separations are up to 251 mV for AA−DA, 126 mV for DA−UA, and 377 mV for UA−AA, which is larger than those at N−PC/GCE (201.3, 125.8, and 327.1 mV) and PC/GCE (188, 118, and 306 mV). The peak potential separation is also much larger than those of many solely N doped carbons.[23−26] Meanwhile, the DPV peak current at N−S−PC/GCE is also explicitly higher than those of other samples. The enlarged separation of peak potential coupled with enhanced peak current indicates that N−S−PC possesses excellent electrocatalytic activity toward oxidation of AA, DA and UA. The extra performance is attributed to the cooperative catalytic effect, which includes highly active sites deriving from N, S dual-doping as well as their good accessibility to reactant benefiting from porous structure. In previous work on N-doped carbons, the catalytic active sites were ascribed mainly to the surrounding C atoms with high positive charge density, deriving from different electronegativity of N and C atoms, while for S doping, the catalytic activity was mainly affected by changed spin density from mismatch of the two elements' orbitals, since the electronegativity of S and C is quite close. Upon N and S dual doping, redistribution of the spin and charge densities may bring a large number of active sites, leading to significantly elevated catalytic activity.[11,27,29] Meanwhile, the porous structure and large pore volume effectively facilitate diffusion of analyte and electrolyte ion, ensuring good accessibility to the catalytic active sites in N−S−PC.[14,23] Apart from this, the hydrogen bonding between N atoms in N−S−PC and target molecules as well as the possible $\pi-\pi$ interactions between hexagonal carbon structure with these molecules may also accelerate charge transfer kinetics.[23,24,26]

The effect of scan rate on CV response of AA, DA, and UA at N−S−PC/GCE was investigated. As shown in Figure S10, the oxidation peak currents of three biomolecules are linear with scan rate (inset plot), indicating a surface-controlled process.[23] The influence of solution pH on peak current and peak potential was also investigated by DPV (Figure S11A). With increasing pH in the range of 4−9, the anodic peak potentials of three molecules shift negatively with linear slopes of 48.7, 67.5, and 68.2 mV/pH, respectively, demonstrating equal numbers of proton and electron transfer for AA, DA, and UA.[33] These oxidation peak currents are found to reach maximum in neutral solution (Figure S11B). For a high sensitivity, pH 7.0 is the optimal selection.

In view of higher sensitivity and better resolution in simultaneous determination, DPV measurements were carried out in PBS (pH 7.0) at N−S−PC/GCE by changing the concentration of target biomolecule while keeping the concentrations of the other two constant. As depicted in Figure 8, upon keeping the concentration of DA and UA at 3 and 4 μM, respectively, the peak current of AA increases proportionally from 50 to 2000 μM with a regression equation of $I_{p,AA}$ (μA) = −0.5725 + 0.0156C_{AA} (μM) (r = 0.9938). Similarly, the peak currents of DA and UA are all proportional in the concentration range of 0.1−50 μM. The linear function is $I_{p,DA}$ (μA) = 3.2177 + 1.3516C_{DA} (μM) (r = 0.9958) and $I_{p,UA}$ (μA) = 2.7398 + 1.3547C_{UA} (μM) (r = 0.9953), respectively. The detection limit (S/N = 3) for AA, DA, and UA is 0.78, 0.02, and 0.06 μM, respectively. The analytical performance of the proposed biosensor was compared with that of the previously developed electrodes (Table 1). The proposed electrode reveals improved performance compared with those in previous reports. In particular, in comparison with the previously developed N-doped carbons,[23−26] N−S−PC exhibits a lower detection limit and wider linear range. N and S dual-doped carbon material with unique porous structure is one of the promising candidates for simultaneous determination of AA, DA, and UA.

Interference, Reproducibility, and Stability. To evaluate the anti-interferential ability of N−S−PC, several possible interferential compounds and ions (including glucose, citric acid, Na_2SO_4, KCl, $ZnCl_2$, $CaCl_2$, and $Mg(NO_3)_2$) were tested. For simultaneous detection of AA (800 μM), DA (5 μM), and UA (20 μM), negligible interferences (signal change below 5%) were found for 100-fold aforementioned compounds and ions, indicating a good selectivity of N−S−PC/GCE.

The reproducibility and stability of N−S−PC/GCE were also evaluated. For 800 μM AA, 5 μM DA, and 20 μM UA, six individual repetitive tests in 0.1 M pH 7.0 PBS at the same electrode showed relative standard deviation (RSD) of 2.2%, 1.2%, and 2.6%, respectively. After 1 week of storage, the current response of UA, DA, AA decayed by 3.2%, 2.5%, and 3.7%, respectively. The above results demonstrate a good reproducibility and stability of the electrode.

CONCLUSION

In summary, a facile strategy for preparing N, S dual doped porous carbon has been proposed by one-step pyrolysis of

cysteine and sodium citrate. By combination of high active sites to small biomolecules deriving from N, S dual doping as well as good accessibility of hierarchical porous carbon, the resulting material displays significantly improved electrocatalytic performance toward oxidation of AA, DA, and UA, manifesting enlarged peak separation and increased peak current. Simultaneous determination of these biomolecules was achieved in a wide concentration range with high sensitivity and selectivity. The prospective application of N−S−PC may be broadened to fuel cells, supercapacitors, and hydrogen storage. Other heteroatoms doped porous carbons with tunable physicochemical properties and versatile applications could be similarly obtained by the modified pyrolytic strategy.

■ ASSOCIATED CONTENT

Supporting Information

SEM and TEM images of PC and N−PC, XRD of N−S−C, textural characteristics and chemical composition of the carbons, EDS and EDS mapping of N−S−PC, high resolution XPS spectra of elements for N−S−C and N−PC, DPVs of individual AA, DA, and UA for various porous carbon materials, CVs and DPVs of coexisting AA, DA, and UA at N−S−C/GCE, and effect of scan rate and pH on electrochemistry of biomolecules. This material is available free of charge via the Internet at http://pubs.acs.org.

■ AUTHOR INFORMATION

Corresponding Author

*E-mail: wbsong@jlu.edu.cn. Fax: +86-431-85168420. Phone: +86-431-85168352.

Author Contributions

The manuscript was written through contributions of all authors. All authors have given approval to the final version of the manuscript.

Notes

The authors declare no competing financial interest.

■ ACKNOWLEDGMENTS

The authors are grateful and thankful for the support of the National Natural Science Foundation of China (Grants 21475051 and 21075048).

■ REFERENCES

(1) Zhang, C.; Mahmood, N.; Yin, H.; Liu, F.; Hou, Y. Synthesis of Phosphorus-Doped Graphene and Its Multifunctional Applications for Oxygen Reduction Reaction and Lithium Ion Batteries. *Adv. Mater.* **2013**, *25*, 4932−4937.

(2) Liu, H.; Liu, Y.; Zhu, D. Chemical Doping of Graphene. *J. Mater. Chem.* **2011**, *21*, 3335−3345.

(3) Shen, W.; Fan, W. Nitrogen-Containing Porous Carbons: Synthesis and Application. *J. Mater. Chem. A* **2013**, *1*, 999−1013.

(4) Jeon, J.-W.; Sharma, R.; Meduri, P.; Arey, B. W.; Schaef, H. T.; Lutkenhaus, J. L.; Lemmon, J. P.; Thallapally, P. K.; Nandasiri, M. I.; McGrail, B. P.; Nune, S. K. In Situ One-Step Synthesis of Hierarchical Nitrogen-Doped Porous Carbon for High-Performance Supercapacitors. *ACS Appl. Mater. Interfaces* **2014**, *6*, 7214−7222.

(5) Zhang, C.; Hao, R.; Liao, H.; Hou, Y. Synthesis of Amino-Functionalized Graphene as Metal-Free Catalyst and Exploration of the Roles of Various Nitrogen States in Oxygen Reduction Reaction. *Nano Energy* **2013**, *2*, 88−97.

(6) Wang, H.; Maiyalagan, T.; Wang, X. Review on Recent Progress in Nitrogen-Doped Graphene: Synthesis, Characterization, and Its Potential Applications. *ACS Catal.* **2012**, *2*, 781−794.

(7) Paraknowitsch, J. P.; Thomas, A. Doping Carbons beyond Nitrogen: An Overview of Advanced Heteroatom Doped Carbons with Boron, Sulphur and Phosphorus for Energy Applications. *Energy Environ. Sci.* **2013**, *6*, 2839−2855.

(8) Kicinski, W.; Szala, M.; Bystrzejewski, M. Sulfur-Doped Porous Carbons: Synthesis and Applications. *Carbon* **2014**, *68*, 1−32.

(9) Zhang, L.; Niu, J.; Li, M.; Xia, Z. Catalytic Mechanisms of Sulfur-Doped Graphene as Efficient Oxygen Reduction Reaction Catalysts for Fuel Cells. *J. Phys. Chem. C* **2014**, *118*, 3545−3553.

(10) Yang, Z.; Yao, Z.; Li, G.; Fang, G.; Nie, H.; Liu, Z.; Zhou, X.; Chen, X.; Huang, S. Sulfur-Doped Graphene as an Efficient Metal-Free Cathode Catalyst for Oxygen Reduction. *ACS Nano* **2012**, *6*, 205−211.

(11) Liang, J.; Jiao, Y.; Jaroniec, M.; Qiao, S. Z. Sulfur and Nitrogen Dual-Doped Mesoporous Graphene Electrocatalyst for Oxygen Reduction with Synergistically Enhanced Performance. *Angew. Chem., Int. Ed.* **2012**, *51*, 11496−11500.

(12) Li, J.; Chen, Y.; Tang, Y.; Li, S.; Dong, H.; Li, K.; Han, M.; Lan, Y.-Q.; Bao, J.; Dai, Z. Metal-Organic Framework Templated Nitrogen and Sulfur Co-Doped Porous Carbons as Highly Efficient Metal-Free Electrocatalysts for Oxygen Reduction Reactions. *J. Mater. Chem. A* **2014**, *2*, 6316−6319.

(13) Niu, X.; Zhao, H.; Chen, C.; Lan, M. Enhancing the Electrocatalytic Activity of Pt−Pd Catalysts by Introducing Porous Architectures. *ChemCatChem* **2013**, *5*, 1416−1425.

(14) Wang, Y.; Jiang, X. Facile Preparation of Porous Carbon Nanosheets without Template and Their Excellent Electrocatalytic Property. *ACS Appl. Mater. Interfaces* **2013**, *5*, 11597−11602.

(15) Qiao, Z.-j.; Chen, M.-m.; Wang, C.-y.; Yuan, Y.-c. Humic Acids-Based Hierarchical Porous Carbons as High-Rate Performance Electrodes for Symmetric Supercapacitors. *Bioresour. Technol.* **2014**, *163*, 386−389.

(16) Liu, Z.; Nie, H.; Yang, Z.; Zhang, J.; Jin, Z.; Lu, Y.; Xiao, Z.; Huang, S. Sulfur−Nitrogen Co-Doped Three-Dimensional Carbon Foams with Hierarchical Pore Structures as Efficient Metal-Free Electrocatalysts for Oxygen Reduction Reactions. *Nanoscale* **2013**, *5*, 3283−3288.

(17) Sevilla, M.; Fuertes, A. B. A General and Facile Synthesis Strategy towards Highly Porous Carbons: Carbonization of Organic Salts. *J. Mater. Chem. A* **2013**, *1*, 13738−13741.

(18) Wei, L.; Lei, Y.; Fu, H.; Yao, J. Fullerene Hollow Microspheres Prepared by Bubble-Templates as Sensitive and Selective Electrocatalytic Sensor for Biomolecules. *ACS Appl. Mater. Interfaces* **2012**, *4*, 1594−1600.

(19) Lakshmi, D.; Whitcombe, M. J.; Davis, F.; Sharma, P. S.; Prasad, B. B. Electrochemical Detection of Uric Acid in Mixed and Clinical Samples: A Review. *Electroanalysis* **2011**, *23*, 305−320.

(20) Liu, A. H.; Wei, M. D.; Honma, I.; Zhou, H. S. Biosensing Properties of Titanate-Nanotube Films: Selective Detection of Dopamine in the Presence of Ascorbate and Uric Acid. *Adv. Funct. Mater.* **2006**, *16*, 371−376.

(21) Zheng, D.; Ye, J.; Zhou, L.; Zhang, Y.; Yu, C. Simultaneous Determination of Dopamine, Ascorbic Acid and Uric Acid on Ordered Mesoporous Carbon/Nafion Composite Film. *J. Electroanal. Chem.* **2009**, *625*, 82−87.

(22) Han, D.; Han, T.; Shan, C.; Ivaska, A.; Niu, L. Simultaneous Determination of Ascorbic Acid, Dopamine and Uric Acid with Chitosan-Graphene Modified Electrode. *Electroanalysis* **2010**, *22*, 2001−2008.

(23) Gai, P.; Zhang, H.; Zhang, Y.; Liu, W.; Zhu, G.; Zhang, X.; Chen, J. Simultaneous Electrochemical Detection of Ascorbic Acid, Dopamine and Uric Acid Based on Nitrogen Doped Porous Carbon Nanopolyhedra. *J. Mater. Chem. B* **2013**, *1*, 2742−2749.

(24) Sheng, Z.-H.; Zheng, X.-Q.; Xu, J.-Y.; Bao, W.-J.; Wang, F.-B.; Xia, X.-H. Electrochemical Sensor Based on Nitrogen Doped Graphene: Simultaneous Determination of Ascorbic Acid, Dopamine and Uric Acid. *Biosens. Bioelectron.* **2012**, *34*, 125−131.

(25) Xiao, C.; Chu, X.; Yang, Y.; Li, X.; Zhang, X.; Chen, J. Hollow Nitrogen-Doped Carbon Microspheres Pyrolyzed from Self-Polymerized Dopamine and Its Application in Simultaneous Electro-

chemical Determination of Uric Acid, Ascorbic Acid and Dopamine. *Biosens. Bioelectron.* **2011**, *26*, 2934−2939.
(26) Zhang, H.; Gai, P.; Cheng, R.; Wu, L.; Zhang, X.; Chen, J. Self-Assembly Synthesis of a Hierarchical Structure Using Hollow Nitrogen-Doped Carbon Spheres as Spacers To Separate the Reduced Graphene Oxide for Simultaneous Electrochemical Determination of Ascorbic Acid, Dopamine and Uric Acid. *Anal. Methods* **2013**, *5*, 3591−3600.
(27) Wohlgemuth, S.-A.; White, R. J.; Willinger, M.-G.; Titirici, M.-M.; Antonietti, M. A One-Pot Hydrothermal Synthesis of Sulfur and Nitrogen Doped Carbon Aerogels with Enhanced Electrocatalytic Activity in the Oxygen Reduction Reaction. *Green Chem.* **2012**, *14*, 1515−1523.
(28) Yan, Y.; Yin, Y.-X.; Xin, S.; Guo, Y.-G.; Wan, L.-J. Ionothermal Synthesis of Sulfur-Doped Porous Carbons Hybridized with Graphene as Superior Anode Materials for Lithium-Ion Batteries. *Chem. Commun.* **2012**, *48*, 10663−10665.
(29) Guo, P.; Xiao, F.; Liu, Q.; Liu, H.; Guo, Y.; Gong, J. R.; Wang, S.; Liu, Y. One-Pot Microbial Method To Synthesize Dual-Doped Graphene and Its Use as High-Performance Electrocatalyst. *Sci. Rep.* **2013**, *3*, 3499.
(30) Li, J.-S.; Li, S.-L.; Tang, Y.-J.; Li, K.; Zhou, L.; Kong, N.; Lan, Y.-Q.; Bao, J.-C.; Dai, Z.-H. Heteroatoms Ternary-Doped Porous Carbons Derived from MOFs as Metal-Free Electrocatalysts for Oxygen Reduction Reaction. *Sci. Rep.* **2014**, 4.
(31) Cui, Z.; Wang, S.; Zhang, Y.; Cao, M. A Simple and Green Pathway toward Nitrogen and Sulfur Dual Doped Hierarchically Porous Carbons from Ionic Liquids for Oxygen Reduction. *J. Power Sources* **2014**, *259*, 138−144.
(32) Matos, I. d. O.; Alves, W. A. Electrochemical Determination of Dopamine Based on Self-Assembled Peptide Nanostructure. *ACS Appl. Mater. Interfaces* **2011**, *3*, 4437−4443.
(33) Yang, L.; Liu, D.; Huang, J.; You, T. Simultaneous Determination of Dopamine, Ascorbic Acid and Uric Acid at Electrochemically Reduced Graphene Oxide Modified Electrode. *Sens. Actuators, B* **2014**, *193*, 166−172.
(34) Liu, Y.; Huang, J.; Hou, H.; You, T. Simultaneous Determination of Dopamine, Ascorbic Acid and Uric Acid with Electrospun Carbon Nanofibers Modified Electrode. *Electrochem. Commun.* **2008**, *10*, 1431−1434.
(35) Dursun, Z.; Gelmez, B. Simultaneous Determination of Ascorbic Acid, Dopamine and Uric Acid at Pt Nanoparticles Decorated Multiwall Carbon Nanotubes Modified GCE. *Electroanalysis* **2010**, *22*, 1106−1114.